astronomy

MDPI

Review

Elastic Polar Oscillations and Nuclear Parameters

Hajime Sotani [1,2,3,4]

[1] Department of Mathematics and Physics, Kochi University, Kochi 780-8520, Japan; sotani@yukawa.kyoto-u.ac.jp
[2] RIKEN Center for Interdisciplinary Theoretical and Mathematical Sciences (iTHEMS), RIKEN, Wako 351-0198, Japan
[3] Co-Creation Organization of Regional Innovation, Kochi University of Technology, Kochi 780-8515, Japan
[4] Theoretical Astrophysics, Institute for Astronomy and Astrophysics Tübingen (IAAT), University of Tübingen, 72076 Tübingen, Germany

Abstract

Owing to the elasticity of a neutron star, the shear and interface modes are excited, in addition to the fundamental, pressure, and gravity modes. While direct observations of the oscillation spectrum remain challenging, potential resonance signatures from these modes could be manifested in the precursors of short gamma-ray bursts from binary neutron star mergers. If the oscillation spectrum is observed, this is a good opportunity to extract the physical properties through the technique of asteroseismology. In particular, we focus on the crustal elasticity and examine the *s*- and *i*-mode frequencies. We find that, for a given EOS specified by the nuclear saturation parameters, the radius-scaled *s*-mode frequencies and the mass-scaled *i*-mode frequencies can be expressed as a function of the stellar compactness, independently of the stiffness of the core EOS, at least when the EOS in a higher-density region can be characterized only by the specific constant sound velocity. Then, we could derive the fitting formula for the s_i-mode for $i = 1$–4 and i_1-mode frequencies as a function of the stellar compactness and the combination of the incompressibility of symmetric nuclear matter, K_0, and the slope parameter for the nuclear symmetry energy, L. If the *s*- and/or *i*-mode oscillation frequencies were observed, one may get the relation between these properties by identifying the observed frequencies with specific modes, using our fitting formula, which offers useful insights into the nuclear saturation parameters and stellar properties. By combining the other observational data, it may be possible to narrow the parameter space of EOS parameters and stellar properties. We emphasize that this article summarizes the results presented in our previous studies and discusses their implications for neutron star seismology.

Keywords: neutron stars; equation of state; asteroseismology

Check for updates

Academic Editor: Brynmor Haskell

Received: 13 October 2026
Revised: 14 November 2026
Accepted: 18 November 2026
Published: 20 November 2026

Copyright: © 2026 by the author. Licensee MDPI, Basel, Switzerland. This article is an open access article distributed under the terms and conditions of the Creative Commons Attribution (CC BY) license.

1. Introduction

Neutron stars are one of the most suitable environments to probe physics under extreme states, where the density inside the star significantly exceeds the nuclear saturation density, and the gravitational and magnetic fields become much stronger than those observed in the Solar System [1,2]. Actually, due to a poor understanding of the properties of high-density matter, the equation of state (EOS) for neutron stars is still uncertain, and as a result, an accurate overall picture of their structure has yet to be established. Thus, the astronomical observations are crucial for revealing the EOS for neutron star matter. In fact, the discoveries of $\sim 2M_\odot$ neutron stars [3–6] have ruled out the soft EOS, with which the expected maximum mass does not reach the observed maximum mass. Also, the observation of the gravitational

waves from the neutron star binary merger, GW170817 [7,8], gives us the upper limit of the tidal deformability for a neutron star, which leads to the constraint on the $1.4M_{\odot}$ neutron star radius being less than 13.6 km [9]. In addition, the X-ray observations of pulse profiles from the rotating neutron stars through the Neutron Star Interior Composition Explorer (NICER) Mission enable us to estimate the mass and radius for PSR J0030+0451 [10,11], for PSR J0740+6620 [12–14], for PSR J0437-4715 [15], and for PSR J0614-3329 [16]. Neutron star models constructed with the true EOS for neutron star matter have to totally satisfy these observational constraints on neutron star mass and radius. In addition to the astronomical constraints mainly on the higher-density region, the terrestrial experiments, e.g., [17–20], and chiral effective field theory [21] are also important for constraining the EOS for the lower-density region.

The neutron star oscillation frequencies are another important piece of information for obtaining the neutron star properties. The frequencies observed in electromagnetic and/or gravitational waves bring us information about the neutron star. In practice, the neutron stars have many kinds of eigenfrequencies, depending on the input physics [22,23]. Since such frequencies strongly depend on the stellar interior properties, once one can find a correlation between a specific frequency and neutron star properties, one can estimate the corresponding properties from the observed frequencies by solving an inverse problem. This technique is known as (gravitational wave) asteroseismology [24–26], which is a similar method to seismology on the Earth or helioseismology on the Sun. For example, by identifying the frequencies of the quasi-periodic oscillations observed from magnetar flares, the crust EOS, mass, and radius of the neutron star have been constrained, e.g., [27–32]. Although gravitational waves from isolated neutron stars have not yet been directly detected, if observed, they may reveal the mass, radius, EOS, and/or rotational properties, e.g., [24,25,33–37]. Furthermore, the technique of gravitational wave asteroseismology has also been adopted even in the protoneutron stars provided via core-collapse supernovae, to understand the explosion mechanism and to extract the physical properties from the gravitational waves, e.g., [38–44]. In a similar way, through the radial oscillation analysis, it has been also reported that the dynamical stability of a hybrid star strongly depends on the timescale of matter changing at the hadron–quark first-order phase transition, which suggests the possibility of the presence of a new class of "slow stable hybrid stars" [45,46].

For considering a realistic neutron star model, one has to take into account the crust elasticity [47], which additionally excites the elastic oscillations, such as torsional oscillations (axial-type modes) and shear (s-) and interface (i-) oscillations (polar-type modes)[1]. The effect of crustal elasticity on neutron star oscillations has been discussed in a series of papers by Bastrukov et al., which laid the foundation for their "Nuclear Elastodynamics" series, in which they pioneered the analytical formulation of the solid crust of a neutron star as an "elastic Fermi continuum" [49–52]. We note that, considering a spherically symmetric stellar model as a background, the polar (even) parity perturbations are completely decoupled from axial (odd) parity ones [53]. The torsional oscillations have been relatively well studied in the context of the identification of the magnetar quasi-periodic oscillations. On the other hand, the studies about the s- and i-modes are very limited (e.g., [54–60]) because the system to solve is more complicated, even though the polar-type oscillations involving the density variations are more important in the gravitational wave astronomy. The crustal torsional oscillations are only excited in the crust (elastic) region, while the s- and i-modes oscillate not inside the crust region but in the whole region of the star, even though the s- and i-modes are excited due to the crust elasticity. So, to discuss the s- and i-modes, one cannot neglect the dependence on the core EOS (or core properties).

The s- and i-modes (as well as the fundamental (f-) and g-modes) may play an important role in the evolution of a binary neutron star. The emission of gravitational waves

causes the orbital frequency to increase, eventually reaching the specific mode frequency of the neutron star in the binary system before merger. In such a moment, the corresponding mode amplitude can be enhanced owing to the energy transfer from the orbital one to the oscillation one due to tidal interactions. This phenomenon is known as tidal excitation, e.g., [61–65], and it is a good opportunity to detect the gravitational waves produced by neutron star oscillations if they occur efficiently. In particular, if these phenomena occur with the crust elastic oscillations, such as the s- and i-modes, the oscillation amplitude enhanced by the tidal interaction eventually breaks the neutron star crust structure, and electromagnetic waves are simultaneously radiated as the X- and/or gamma-ray burst. This is known as resonant shattering [66–69]. If it occurs, the precursor signal resulting from the resonant shattering would be observed before the main short gamma-ray burst corresponding to the merger of the binary neutron star, which may offer information on the stellar oscillation spectra. Since the i-mode frequencies are typically ∼10–100 Hz [66,67], which are lower than the s-mode frequencies, they easily match the orbital frequencies before merger. That is, the i-modes may be more relevant in the observations of resonant shattering. Observationally, the precursors have been detected 1–10 s before the main flare is detected [70,71], and moreover, a candidate of quasi-periodic oscillation with ∼22 Hz has also been discovered in the precursor associated with GRB 211211A [72]. Anyway, once one observes the precursor signal due to the resonant shattering and identifies it with the i- or s-mode oscillations, it helps us to extract the crustal properties [58,59,73,74].

Nevertheless, the oscillation frequencies excited in a neutron star strongly depend on the neutron star properties. Namely, without understanding such dependencies, it may be difficult to extract the physical information from the (gravitational wave) frequencies, even if they are observed. One possibility to solve this model dependence is a universal relation between the frequencies and neutron star properties, independent of the model parameters, such as the EOS. In fact, several universal relations (or empirical relations) are proposed, e.g., [24,25,37,75–80][2]. So, in this article, to derive the fitting formula for estimating the s- and i-mode frequencies, we systematically examine the dependence of their frequencies on the neutron star properties and EOS.

This article summarizes the results presented in Refs. [58–60] and discusses their implications for neutron star seismology. This article is organized as follows. In Section 2, we describe the neutron star models focusing on the crustal region and also the shear modulus characterizing the crust's elasticity. Then, in Section 3, we discuss the behavior of the s- and i-mode frequencies and their dependence on the EOS parameters, and derive the fitting formula for expressing them. In this section, we also discuss the accuracy of the Cowling approximation, which is the approximation that the metric perturbations are neglected, in the s- and i-mode frequencies. Finally, we conclude this study in Section 4. Unless otherwise mentioned, we adopt geometric units with $c = G = 1$, where c and G denote the speed of light and the gravitational constant, and use the metric signature $(-,+,+,+)$.

2. Neutron Star Equilibrium and Shear Modulus

As a background model for the elastic oscillations, we consider a static, strain-free, and spherically symmetric stellar model, which is described with the metric given by

$$ds^2 = -e^{2\Phi}dt^2 + e^{2\Lambda}dr^2 + r^2\left(d\theta^2 + \sin^2\theta d\phi^2\right), \tag{1}$$

where Φ and Λ are metric functions that depend only on the radial coordinate r, and Λ is directly associated with the mass function $m(r)$ through $e^{-2\Lambda} = 1 - 2m/r$. We note that the mass function is the gravitational mass enclosed within the radius r. The stellar equilibrium is constructed by integrating the Tolman–Oppenheimer–Volkoff (TOV) equations, adopting

an appropriate EOS. To systematically examine the dependence of the elastic oscillation frequencies on the nuclear parameters, we adopt a phenomenological EOS proposed by Oyamatsu and Iida [83,84] (hereafter referred to as OI-EOS).

The bulk energy, w, of zero-temperature nuclear matter constructed with any EOS can be expanded in the vicinity of the saturation density, n_0, of the symmetric nuclear matter, whose proton number density, n_p, is the same as the neutron number density, n_n, as a function of the baryon number density, n_b, and the neutron excess, δ:

$$w = w_0 + \frac{K_0}{2}u^2 + O(u^3) + \left[S_0 + Lu + O(u^2)\right]\delta^2, \tag{2}$$

where $u \equiv (n_\mathrm{b} - n_0)/(3n_0)$ and $\delta \equiv (n_n - n_p)/n_\mathrm{b}$. The coefficients in this expansion, w_0, n_0, K_0, S_0, and L, are the nuclear saturation parameters, which characterize each EOS. We note that, although we consider the expansion as in Equation (2) in this study, one can also expand into higher-order terms and discuss the additional nuclear saturation parameters. Additionally, since the fourth-order symmetry energy at saturation density, i.e., the term proportional to δ^4, is typically much smaller than the quadratic term, the empirical parabolic approximation is known to work well around nuclear saturation density [85,86]. Among the five expansion parameters in Equation (2), w_0, n_0, and S_0 are more constrained from the terrestrial experiments due to the saturation properties of nuclear matter, while the remaining parameters, K_0 and L, are more difficult to constrain from the experiments. This is because one has to obtain the data in a relatively wider density region around the saturation density to constrain the values of K_0 and L. The fiducial values of K_0 and L obtained from the experiments are $K_0 = 240 \pm 20$ MeV [87] and $L = 60 \pm 20$ MeV [88,89], and it is also possible to constrain them via astronomical observations, e.g., [30,90–92].

The OI-EOS is constructed for given values of K_0 and L so that the bulk energy becomes the form given by Equation (2) in the limit of $\delta \to 0$ and $n_\mathrm{b} \to n_0$, and the other saturation parameters are tuned to reproduce the empirical nuclear data for stable nuclei adopting a simplified version of the extended Thomas–Fermi theory [83,84]. Thus, the neutron star properties in relatively lower-density regions can be well described using the OI-EOS, while the discussion in higher-density regions with the OI-EOS may be insufficient. Therefore, to see the dependence on the stiffness of the EOS in a higher-density region, we also consider the EOS for $\varepsilon \geq \varepsilon_t$ characterized by the sound velocity, c_s, assuming that $c_s = (dp/d\varepsilon)^{1/2}$ in this study, i.e.,

$$p = \alpha(\varepsilon - \varepsilon_t) + p_t, \tag{3}$$

where ε and p denote the energy density and pressure; $\alpha = c_s^2$; and ε_t and p_t are the transition density and the pressure at $\varepsilon = \varepsilon_t$, which is connected to the OI-EOS at $\varepsilon = \varepsilon_t$.

Based on chiral effective field theory for low-energy nuclear forces, the EOS of pure neutron matter has been precisely determined with well-quantified theoretical uncertainties up to approximately twice the saturation density [93]. This provides a rigorous foundation for constructing the neutron star EOS, a framework further validated by terrestrial experiments measuring collective flows in heavy-ion collisions [94], so that the density region up to this point is widely adopted as a well-established anchor in recent studies of the neutron star EOS [95], although heavy-ion collision data are notoriously very dependent on transport models used in the analysis. Therefore, in this study, we assume that ε_t is equal to twice the saturation density. Considering that the transition density between the crust and core is roughly one-third to one-half of the saturation density [84,96], the crust region is well expressed by only the OI-EOS. Hereafter, unless the value of α is specified, the stellar structures are constructed using the original OI-EOS by integrating the TOV equations from the center to the surface.

The OI-EOS tells us the transition density from the crust to the core (and also the transition densities where the various nuclear pasta structures appear), which mainly depends

on L; i.e., the transition density to the core region becomes larger as L decreases [83,84]. The thickness of the pasta region also becomes thicker as L decreases, while the pasta structure disappears when $L \gtrsim 100$ MeV [84]. On the other hand, the determination of the density at the crust outer surface, i.e., the transition density between the crust and envelope, is more difficult [47,97–99]. This is because one has to take into account the physical temperature effect on the matter properties when the density becomes much lower than the saturation density. Namely, one can generally consider a zero-temperature neutron star model even though the physical temperature is around 10^8 K, because the Fermi temperature is much higher than the physical temperature inside the neutron star. Meanwhile, in the vicinity of the stellar surface, where the density becomes much lower than the nuclear saturation density, the Fermi temperature also becomes low, and one cannot neglect the effect of the temperature. In practice, the density of the crust outer surface becomes $\sim 10^6$–10^{10} g/cm^3 [97,100]. In this study, we simply assume that this transition density is 10^{10} g/cm^3, while the stellar surface density is 10^6 g/cm^3. How the i-mode frequencies shift due to the change in the transition density between the crust and the envelope is discussed in Appendix B, using a simple model. In the left panel of Figure 1, as an example, we show the radial profile of the energy density for the neutron star model with $1.4M_\odot$ and 12.4 km, adopting the OI-EOS with $K_0 = 230$ and $L = 73.4$ MeV. From this figure, one observes that the crust thickness is very tiny compared to the stellar radius, and also that most of the crust region is composed of spherical nuclei, and the pasta layer is very narrow.

The crust elasticity is characterized by the shear modulus, μ. In a phase consisting of spherical nuclei arranged in a body-centered cubic (bcc) lattice, which occupies most of the crust region, the shear modulus, $\mu_{\rm sp}$, is formulated as

$$\mu_{\rm sp} = 0.1194 \frac{n_i (Ze)^2}{a}, \tag{4}$$

where n_i, Z, and a denote the ion number density, the ion charge number, and the Wigner–Seitz cell radius, i.e., $n_i = (4\pi a^3/3)^{-1}$ [101,102]. This shear modulus has been derived under the assumption that the ion is a point particle. On the other hand, although the study of elasticity in the phases of cylindrical and slab-like nuclei may be poor, as per the study by Pethick and Potekhin [103], the shear modulus in the cylindrical phase is expressed as

$$\mu_{\rm cy} = \frac{2}{3} E_{\rm Coul} \times 10^{2.1(w_2 - 0.3)}, \tag{5}$$

using the Coulomb energy per volume of a Wigner–Seitz cell, $E_{\rm Coul}$, and the volume fraction of cylindrical nuclei, w_2, while the phase of slab-like nuclei behaves as a fluid against the linear response; i.e., the shear modulus in this phase is considered as

$$\mu_{\rm sl} = 0, \tag{6}$$

when one considers the linear analysis. Furthermore, the shear moduli inside the phases of cylindrical-hole nuclei and spherical-hole nuclei are estimated with the formulae given by Equations (5) and (4), because the structure is the same as that of the phases of cylindrical and spherical nuclei, respectively. Then, as shown in the right panel of Figure 1, one can derive the shear moduli inside the crust region, depending on the various phases. That is, the crustal structure consists of two elastic regions separated by a fluid phase composed of slab-like nuclei [30].

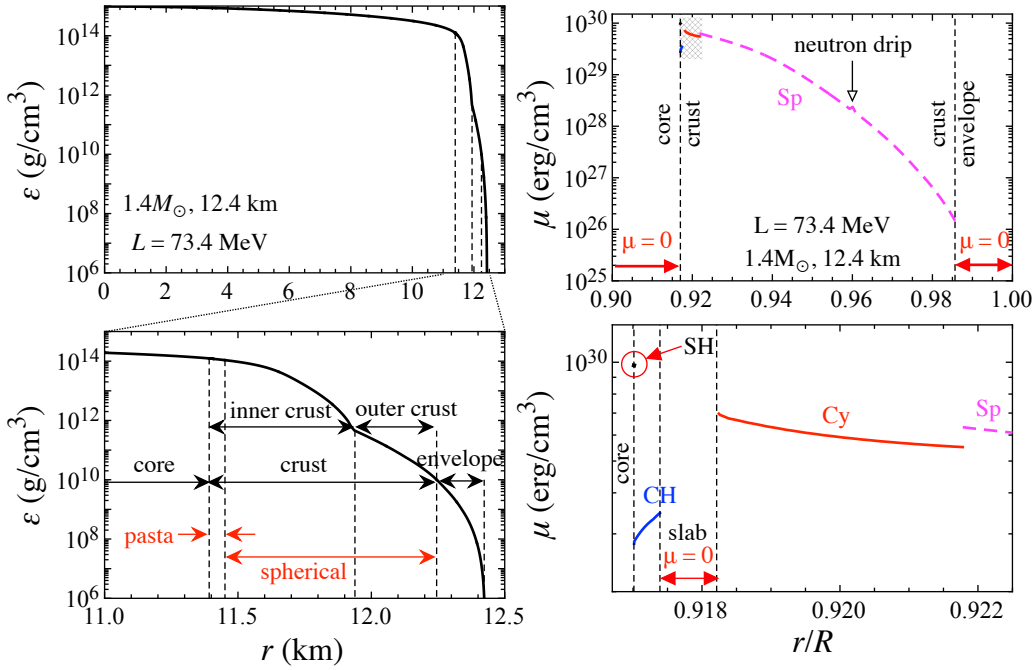


Figure 1. (**Left**) panel: radial profile of energy density inside the neutron star with $1.4M_\odot$ and 12.4 km, adopting the EOS with $K_0 = 230$ and $L = 73.4$ MeV. The bottom panel is an enlarged view of the region for $r \geq 11$ km. The vertical dashed lines in the top panel denote the boundary between the core and crust, the boundary between the inner and outer crust, and the boundary between the crust and envelope, from left to right. (**Right**) panel: the radial distribution of the shear modulus, depending on the various nuclear shapes, i.e., sphere (Sp), cylindrical (Cy), cylindrical-hole (CH), and spherical-hole (SH), for the same neutron star model as on the left. The bottom panel is an enlarged view of the shaded region in the top panel. Taken from Ref. [58].

Before we start to discuss the oscillation frequencies, we have to emphasize the limitation of our EOS models. The nuclear saturation parameters, which are the lowest order of the expansion coefficients, w_0, n_0, K_0, S_0, and L, characterize (zero-temperature) homogeneous nuclear matter around the saturation point of symmetric matter, while the neutron star crust contains highly asymmetric and inhomogeneous matter over a broad range of sub-saturation densities. Its composition, crust–core transition, and elastic properties depend not only on the nuclear saturation parameters but also on higher-order density and isospin dependences, nuclear surface properties, and other finite-size contributions. Although the variations of these additional properties are likely to be correlated with variations of the nuclear saturation parameters within a particular nuclear parametrization, such correlations are not necessarily preserved when the additional nuclear-functional parameters are independently varied, e.g., [104]. A similar issue arises because nuclear matter parameters alone do not fix the EOS across the full density range. In practice, how nuclear-functional uncertainties can be propagated beyond a restricted parametrization is discussed, e.g., [105], which develops a flexible nuclear EOS that allows fixing a broad range of nuclear matter parameters, with a consistent treatment of the crust and core. That is, a different nuclear EOS with comparable or even identical values of K_0 and L can produce very different stellar properties, and therefore mode frequencies. That is, the small residuals of the fitting formulae derived within the OI family considered in this article should not be interpreted as demonstrating comparably small uncertainties in the nuclear parameters inferred from future observations. Considering these points, since we consider EOS models characterized by the nuclear saturation parameters in this article, our statement is valid only when the correlations with the nuclear saturation parameters are well preserved. If not, additional analysis is needed to validate our statement.

3. Oscillations Excited by the Crust Elasticity

To determine the oscillation frequencies, we simply assume the Cowling approximation in this study. That is, we consider the fluid motion on the fixed metric. Even with such an approximation, one can qualitatively discuss the behavior of frequencies [106,107]. In this case, the perturbation equations are derived from the linearized energy–momentum conservation law, i.e., $\delta\left(\nabla_\mu T^{\mu\nu}\right) = \nabla_\mu \delta T^{\mu\nu} = 0$, where the first equality holds because of the Cowling approximation. Then, by imposing the appropriate boundary conditions at the center and surface and the junction conditions at the interfaces between the elastic and anelastic regions[3], the problem to solve becomes an eigenvalue problem with respect to the eigenvalue ω. Once ω is determined, the eigenfrequencies, f, are obtained from the resultant ω via $f = \omega/(2\pi)$. The concrete perturbation equations, the imposed boundary conditions, and the imposed junction conditions are shown in Refs. [55,58]. We note that one can obtain all eigenfrequencies, such as the f-, pressure (p-), s-, and i-modes, excited in the current model from the same system of equations. We note that the g-modes cannot be excited in our model due to the assumption of $c_s^2 = dp/d\varepsilon$. In this study, we particularly focus only on the $\ell = 2$ modes, because they are dominant modes in gravitational radiation [22,108].

We note that if some of the dripped neutrons behave as a superfluid, which does not contribute to the effective inertia participating in the elastic oscillations, the s- and i-mode frequencies may increase compared to those without such effects, analogous to the crustal torsional oscillations [109]. In addition, as mentioned in the following Section 3.1, the number of the i-modes excited in the neutron star without the composition gradient is equivalent to the number of interfaces where the elasticity becomes zero [56]. So, if $\mu_{\rm sl}$ has a tiny value instead of zero, different from our simple approximation, the number of interfaces changes from 4 to 2. In such a case, the i-modes are excited only at the boundaries between the crust and envelope and between the crust and core. Furthermore, in such a case, the junction conditions adopted in the integration of the perturbation equations are also changed, so that the s-mode frequencies may also be shifted.

Furthermore, recent work by Gao et al. [48] has shown that, in neutron star models with stratification, the standard crust-core interface modes disappear and are replaced by modes in which gravitational and interface properties are intermingled. In other words, the mode spectrum itself can change as a result of the layered structure. On the other hand, this paper assumes that $c_s^2 = dp/d\varepsilon$; as a result, the g-mode arising from composition no longer exists. It should therefore be noted that if composition gradients that induce the g-mode oscillations are taken into account, the i-mode discussed here may disappear.

3.1. Behavior of the s- and i-Modes

Before discussing the fitting formula, we show the behavior of the eigenfunctions of the s- and i-mode oscillations. Both modes are excited by the elasticity inside the star. The number of s-modes is infinite, just like that of the p-modes. The lowest mode has one node in the eigenfunction, and the nodal number increases as the mode frequency becomes higher. Using the nodal number, i, the mode is identified as the s_i-mode. In Figure 2, the eigenfunction of the Lagrangian displacement in the angular direction, V, for the s_i-modes with $i = 1$–5 is shown as a function of the normalized radial coordinate, r/R, focusing on the crust region. From this figure, one observes that the s-mode oscillations are almost confined inside the elastic region. At the boundary between the anelastic and elastic regions, V becomes discontinuous, while the Lagrangian displacement in the radial direction, W, becomes continuous owing to the junction condition at the same boundary. Since the

s_i-modes with i nodes are confined inside the elastic region, one can roughly estimate the wavelength of the s_i-mode (λ_i) with the thickness of the elastic region, ΔR:

$$\lambda_i \approx 2\Delta R/i. \tag{7}$$

Therefore, the frequency of the s_i-mode is also estimated as

$$f_{s_i} \approx v_s/\lambda_i, \tag{8}$$

where v_s denotes the shear velocity, i.e., the propagation speed of elastic oscillations. Since we only focus on the frequency region less than a few kHz in this study, we can only find the s-mode oscillations excited in the phase of spherical and cylindrical nuclei, as shown in Figure 2. In addition to the s-mode we found, the s-mode can also be excited inside the phase of cylindrical-hole and spherical-hole nuclei, which is another elastic region inside the star. That may be so, but the thickness of the phase of cylindrical-hole and spherical-hole nuclei, $\Delta R_{\rm CHSH}$, is much smaller than that of the phase of spherical and cylindrical nuclei, $\Delta R_{\rm SpCy}$, e.g., $\Delta R_{\rm CHSH}/\Delta R_{\rm SpCy} \lesssim 10^{-2}$. That is, as per the above rough estimation, the s-mode frequencies excited in $\Delta R_{\rm CHSH}$, $f_s^{\rm (CHSH)}$, become much higher than the s-mode frequencies excited in $\Delta R_{\rm SpCy}$, $f_s^{\rm (SpCy)}$; e.g., $f_s^{\rm (CHSH)}$ may be higher than ∼50 kHz (likely of no interest to current gravitational wave detectors), considering that $f_s^{\rm (SpCy)}$ is typically higher than ∼500 Hz.

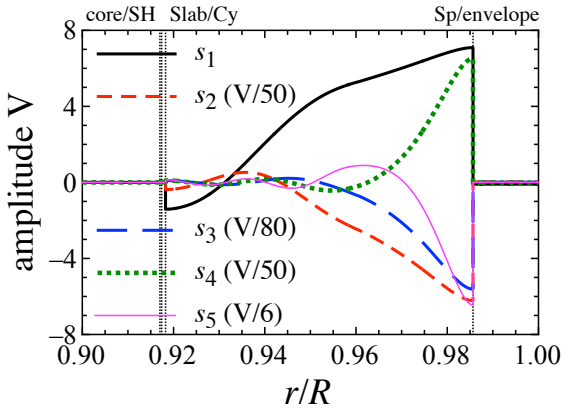


Figure 2. Radial profile of the eigenfunction of the Lagrangian displacement in the angular direction, V, for the s_i-modes with i = 1–5 for the neutron star model with $1.4M_\odot$ and 12.4 km, adopting the EOS with $K_0 = 230$ and $L = 73.4$ MeV. The vertical lines from right to left denote the boundary between the crust and the envelope (Sp/envelope), the boundary between the phases composed of cylindrical and slab-like nuclei (Slab/Cy), the boundary between the phases of slab-like and cylindrical-hole nuclei (CH/Slab), and the boundary between the phase composed of spherical-hole nuclei and the core (core/SH). Taken from Ref. [58].

Unlike the number of the s-modes, the number of the i-modes is finite. How many of the i-modes can be excited in a neutron star corresponds to the number of interfaces between the phases with zero and nonzero elasticity [56]. Since the stellar model considered in this study has four interfaces, i.e., between the envelope and the phase of spherical nuclei, between the phases of cylindrical and slab-like nuclei, between the phases of slab-like and cylindrical-hole nuclei, and between the phase of spherical-hole nuclei and the core region, four interface modes can be excited[4]. In addition, unlike the s-modes, since there is no established convention for numbering the subscript of the i_i-modes, we will number them here in order of decreasing frequency, starting with $i = 1, 2, \cdots$. As an example, Figure 3 shows the radial profile of the amplitude of W and V for the i_i-mode oscillations with i = 1–4, where the vertical lines denote the interfaces between the elastic and anelastic

regions. From the figure, one can observe that, just like in the *s*-mode oscillations, due to the junction condition at the interface, W is continuous while V is discontinuous at the interfaces. The amplitude of W increases significantly at the interface, while V almost behaves like a step function that is discontinuous at the interface. In addition, unlike that of the *s*-modes, the amplitude of the *i*-mode in the anelastic region becomes comparable to that in the elastic region.

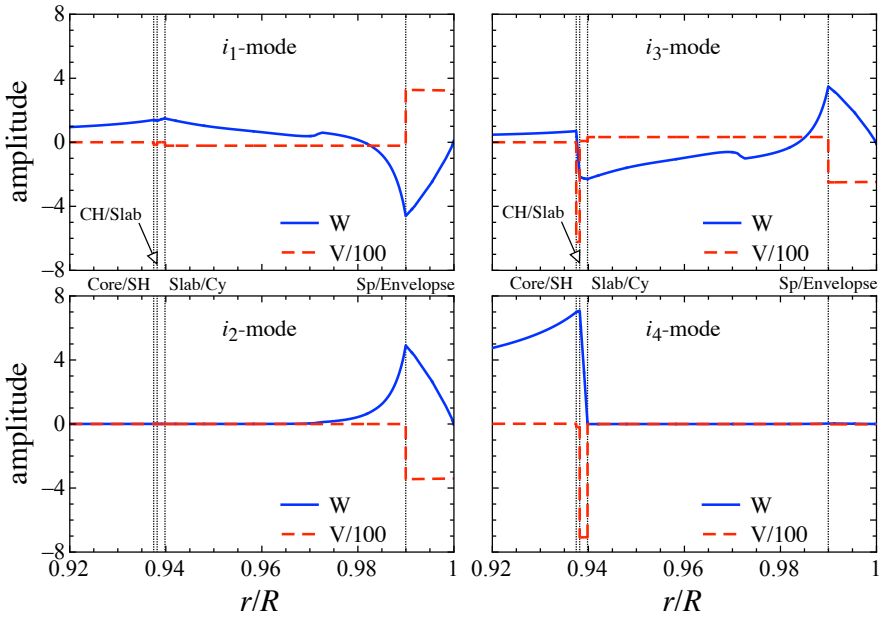


Figure 3. Radial profile of the eigenfunctions of W and V for the i_i-modes with $i = 1$–4 for the neutron star model with $1.44M_\odot$ and 10.2 km, adopting the EOS with $K_0 = 230$ and $L = 42.6$ MeV. The meaning of the vertical lines is the same as in Figure 2. Taken from Ref. [59].

3.2. Fitting Formula

The torsional oscillations, which are the axial-type oscillations excited by the presence of elasticity, do not involve the stellar deformation, and they are confined inside the elastic region. So, one can discuss the frequencies of the torsional oscillations independently of the core region once one can construct the equilibrium model of the neutron star crust. On the other hand, the *s*- and *i*-modes are also the oscillation modes excited by the elasticity, but they are the polar-type oscillations, which involve the radial motion. Thus, for discussing the *s*- and *i*-mode oscillations, one has to take into account not only the crust properties but also the core properties. In fact, even if one adopts the EOS with the same saturation parameters, i.e., the lower-density region is described in the same way, the frequencies of the polar oscillations are shifted, depending on the core EOS (or core properties). To see such a dependence of the frequencies on the core properties, as mentioned in Section 2, we examine the frequencies by changing the stiffness of the core EOS, characterizing its sound velocity, as in Equation (3). As an example, we consider the stellar models constructed with the OI-EOS with $L = 42.6$ MeV and 73.4 MeV, fixing $K_0 = 230$ MeV, and those with the same OI-EOS connected to the EOS given by Equation (3) with $\alpha = 1/3$, 0.6, and 1. The mass and radius of the resultant neutron stars are shown in Appendix A.

Then, as shown in Figure 4, we find that the radius-scaled s_i-mode frequencies, $f_{s_i}R$, and the mass-scaled i_i-mode frequencies, $f_{i_i}M$, are well expressed as a function of the stellar compactness, independently of the stiffness of the core EOS, at least when the core EOS can be characterized only by the specific constant sound velocity. From this figure, we can derive

the fitting formulae for $f_{s_i}R$ and $f_{i_i}M$ as a function of $\chi \equiv M_{1.4}/R_{12}$ with the normalized mass, $M_{1.4} \equiv M/(1.4M_\odot)$, and radius, $R_{12} \equiv R/(12\ \mathrm{km})$, such as

$$f_{s_i}R\ (\mathrm{kHz\ km}) = a_{0i} + a_{1i}\chi, \tag{9}$$

$$f_{i_i}M\ (\mathrm{kHz}\ M_\odot) = b_{0i} + b_{1i}\chi + b_{2i}\chi^2, \tag{10}$$

where a_0, a_1, b_0, b_1, and b_2 are adjusting coefficients, depending on the saturation parameters. This result suggests that one may be able to evaluate the nuclear saturation parameters from observations of s- and/or i-mode frequencies, together with an additional observational constraint on the neutron star mass and radius, even without knowledge of the core EOS.

Furthermore, we attempt to express the adjusting coefficients in Equations (9) and (10) as a function of the saturation parameters, which partially succeeds [59]. To derive such a fitting formula for the s- and i-mode frequencies, we examine the dependence of the adjusting coefficients on the saturation parameters, adopting the OI-EOS with 6 different sets of K_0 and L, i.e., $(K_0, L) = (180, 31.0)$, $(180, 52.2)$, $(230, 23.7)$, $(230, 42.6)$, $(230, 73.4)$, and $(360, 40.9)$ in the unit of MeV. Then, after much trial and error, we find that the adjusting coefficients in Equation (9) can be well expressed as a function of the specific combination of the saturation parameters, K_0 and L, expressed as y_{0i} and y_{1i}, which depend on the nodal number i for the s_i-modes, as

$$a_{0i} = a_{0i}^{(0)} + a_{0i}^{(1)}\left(\frac{y_{0i}}{100\ \mathrm{MeV}}\right) + a_{0i}^{(2)}\left(\frac{y_{0i}}{100\ \mathrm{MeV}}\right)^2, \tag{11}$$

$$a_{1i} = a_{1i}^{(0)} + a_{1i}^{(1)}\left(\frac{y_{1i}}{100\ \mathrm{MeV}}\right) + a_{1i}^{(2)}\left(\frac{y_{1i}}{100\ \mathrm{MeV}}\right)^2, \tag{12}$$

where y_{0i} and y_{1i} are listed in Table 1, and the coefficients in Equations (11) and (12), i.e., $a_{0i}^{(j)}$ and $a_{1i}^{(j)}$ for $j = 0, 1, 2$, are listed in Table 2. In a similar way, the adjusting coefficients in Equation (10) are also fitted as a function of the specific combination of K_0 and L expressed as

$$b_{ji} = b_{ji}^{(0)} + b_{ji}^{(1)}\left(\frac{z_{ji}}{100\ \mathrm{MeV}}\right) + b_{ji}^{(2)}\left(\frac{z_{ji}}{100\ \mathrm{MeV}}\right)^2, \tag{13}$$

$$b_{j4} = b_{j4}^{(0)} + b_{j4}^{(1)}\left(\frac{z_{j4}}{100\ \mathrm{MeV}}\right)^{-1} + b_{j4}^{(2)}\left(\frac{z_{j4}}{100\ \mathrm{MeV}}\right)^{-2}, \tag{14}$$

for $j = 0, 1, 2$ and $i = 1, 2, 3$, where z_{ji} denotes L or the combination of K_0 and L depending on j and i, which are listed in Table 1, even though the fitting for the i_3- and i_4-mode frequencies does not work well, as seen below, and the coefficients in Equations (13) and (14), i.e., $b_{ji}^{(k)}$ for $j = 0, 1, 2$ and $k = 0, 1, 2$, are listed in Table 3.

Table 1. Specific combinations of K_0 and L (y_{0i} and y_{1i}) in the fitting of a_{0i} and a_{1i} expressed by Equations (11) and (12), and the specific combinations of K_0 and L (z_{ji} for $i = 1, 2, 3, 4$ and $j = 0, 1, 2$) in the fitting of b_{0i}, b_{1i}, and b_{2i}, given by Equations (13) and (14).

i	y_{0i}	y_{1i}	z_{0i}	z_{1i}	z_{2i}
1	$(K_0^4L^5)^{1/9}$	$(K_0^5L^6)^{1/11}$	$(K_0^2L^3)^{1/5}$	L	L
2	$(K_0L^6)^{1/7}$	$(K_0L)^{1/2}$	$(K_0^3L)^{1/4}$	$(K_0^4L)^{1/5}$	$(K_0^9L)^{1/10}$
3	$(K_0L^3)^{1/4}$	$(K_0L)^{1/2}$	L	L	L
4	$(K_0^4L^5)^{1/9}$	$(K_0L)^{1/2}$	$(K_0^3L)^{1/4}$	$(K_0^2L)^{1/3}$	$(K_0^2L)^{1/3}$

Table 2. Coefficients $a_{0i}^{(j)}$ and $a_{1i}^{(j)}$ for $j = 0, 1, 2$ in the fitting of a_{0i} and a_{1i} expressed by Equations (11) and (12).

i	$a_{0i}^{(0)}$	$a_{0i}^{(1)}$	$a_{0i}^{(2)}$	$a_{1i}^{(0)}$	$a_{1i}^{(1)}$	$a_{1i}^{(2)}$
1	1.8624	−0.2316	−0.1364	9.4614	0.7380	−2.1114
2	1.5724	2.5259	−2.1216	17.8859	−3.0316	−1.0974
3	3.8459	−3.8269	2.3209	18.4672	3.3390	−3.6406
4	3.5630	2.0388	−2.1046	28.7034	−8.3357	1.0013

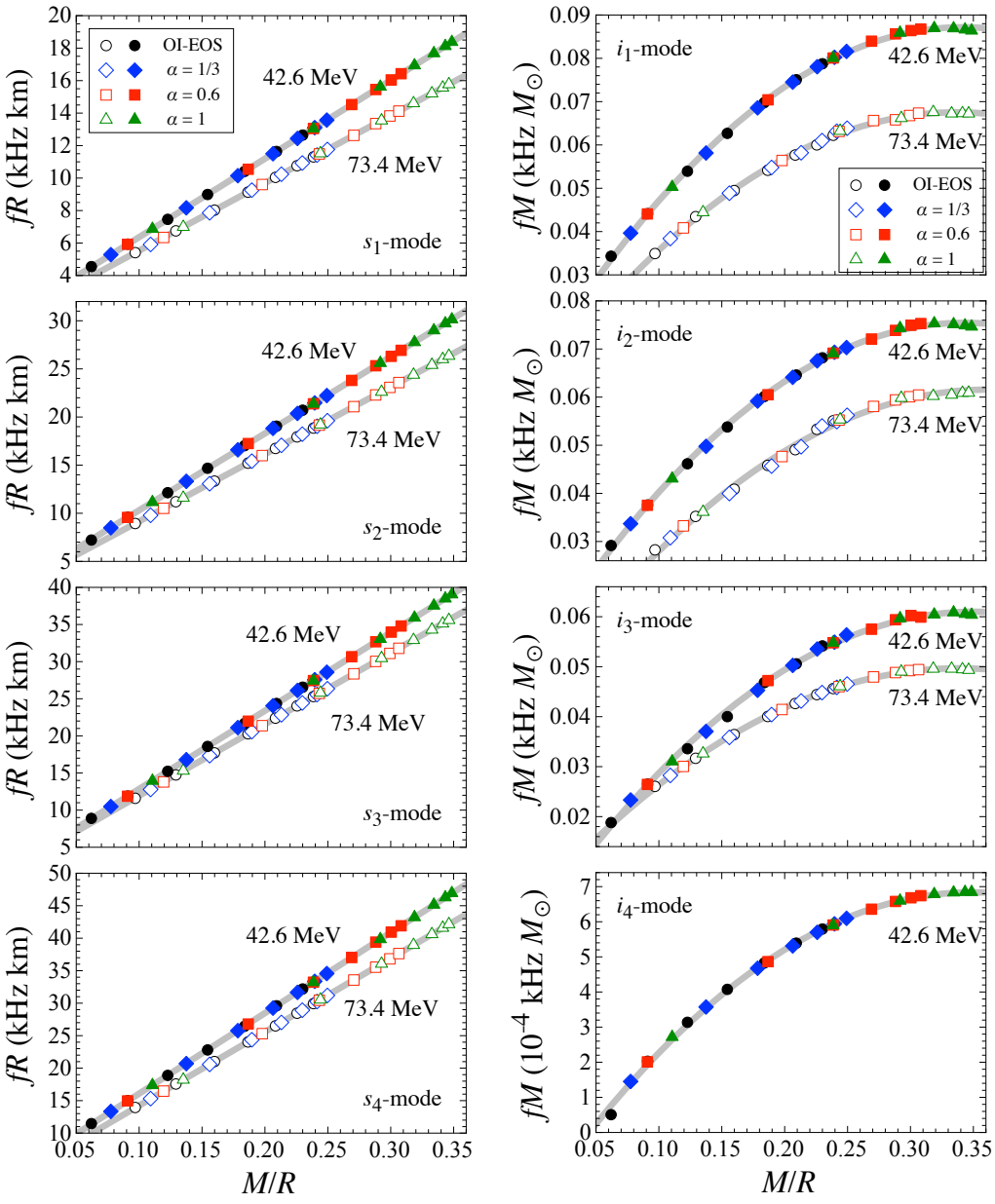


Figure 4. For neutron star models constructed using the EOS with $L = 42.6$ and 73.4 MeV, fixing $K_0 = 230$ MeV, and with different core EOS stiffness, $\alpha = c_s^2$, the radius-scaled s_i-mode frequencies in the left panels and the mass-scaled i_i-mode frequencies in the right panels are shown as a function of the stellar compactness, M/R. The thick solid lines denote the fitting formulae given by Equation (9) in the (**left**) panel and Equation (10) in the (**right**) panel. Taken from Ref. [58].

To check how well our fitting formulae work, we calculate the relative deviation, Δ, of the frequencies from those evaluated with the fitting formulae, as

$$\Delta \equiv \frac{|f - f_{\rm em}|}{f}, \tag{15}$$

where f and $f_{\rm em}$ respectively denote the frequencies determined by numerically solving the eigenvalue problem and those evaluated with the fitting formulae given by Equations (9), (11) and (12) for the s_i-modes and Equations (10), (13) and (14) for the i_i-modes, and show them in Figure 5 for the s_i-modes and in Figure 6 for the i_i-modes, respectively. From Figure 5, we find that our fitting formulae work well for the s_i-mode frequencies with less than ∼1% error, except for the unrealistic low-mass neutron stars. Meanwhile, as shown in Figure 6, using our fitting formulae, the i_1- and i_3-mode frequencies can be evaluated within a few % and ∼10% accuracy, respectively, but the i_2- and i_4-mode frequencies are evaluated only to within an order of magnitude due to the weak correlations with nuclear saturation parameters. We note that we derive the fitting formulae for the s- and i-mode frequencies using the specific combination of K_0 and L listed in Table 1, but this is not unique, and better-fitting formulae may exist.

Table 3. Coefficients $b_{ji}^{(k)}$ for $j = 0, 1, 2$ and $k = 0, 1, 2$ in the fitting of b_{0i}, b_{1i}, and b_{2i} with Equations (13) and (14).

i	$b_{0i}^{(0)}$	$b_{0i}^{(1)}$	$b_{0i}^{(2)}$	$b_{1i}^{(0)}$	$b_{1i}^{(1)}$	$b_{1i}^{(2)}$	$b_{2i}^{(0)}$	$b_{2i}^{(1)}$	$b_{2i}^{(2)}$
1	0.0038337	0.0073437	−0.0068798	0.083392	−0.042113	0.024719	−0.020817	0.010515	−0.0069116
2	0.016178	−0.019248	0.0048505	0.048374	0.010393	−0.0017163	−0.0088285	−0.0040927	0.00056104
3	0.02413	−0.053581	0.033518	0.1714	−0.2740	0.1446	−0.040238	0.059085	−0.028536
4	0.0017045	−0.0071152	0.0062548	0.018248	−0.049949	0.034971	−0.0045017	0.012316	−0.0086167

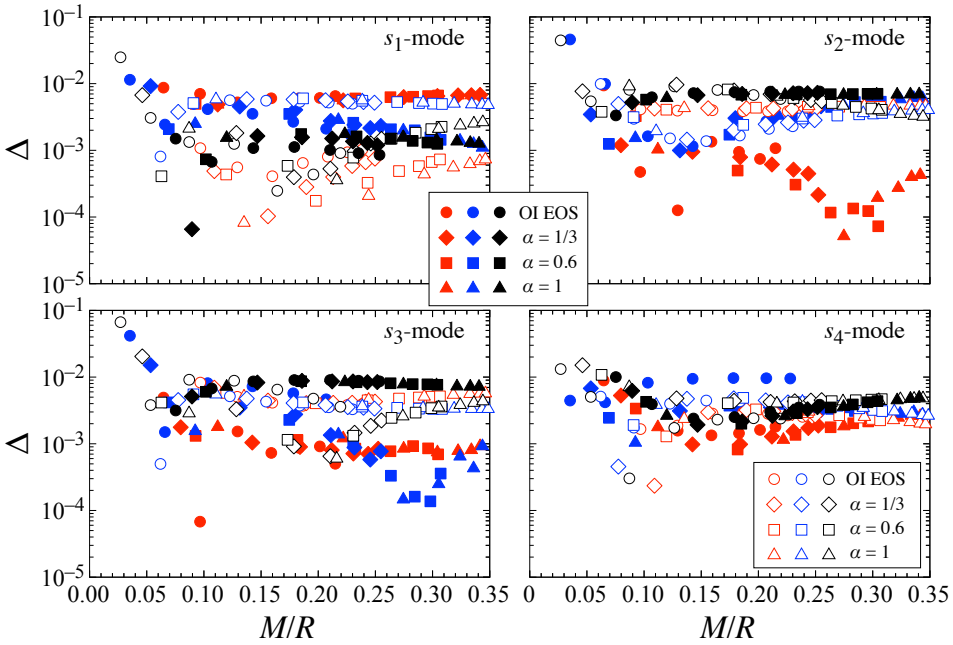


Figure 5. For the s_i-mode frequencies with $i = 1$–4, the relative deviation of the frequencies determined by solving the eigenvalue problem from those evaluated with the fitting formulae given by Equations (9), (11) and (12) is shown as a function of the stellar compactness, M/R, for the various stellar models constructed with different saturation parameters and stiffness of the core EOS. The circles, diamonds, squares, and triangles denote the different stiffness of the core EOS, i.e., original OI-EOS (circles), $\alpha = 1/3$ (diamonds), $\alpha = 0.6$ (squares), and $\alpha = 1$ (triangles). The different colors and whether marks are open or filled denote the EOS models with different saturation parameters. Taken from Ref. [59].

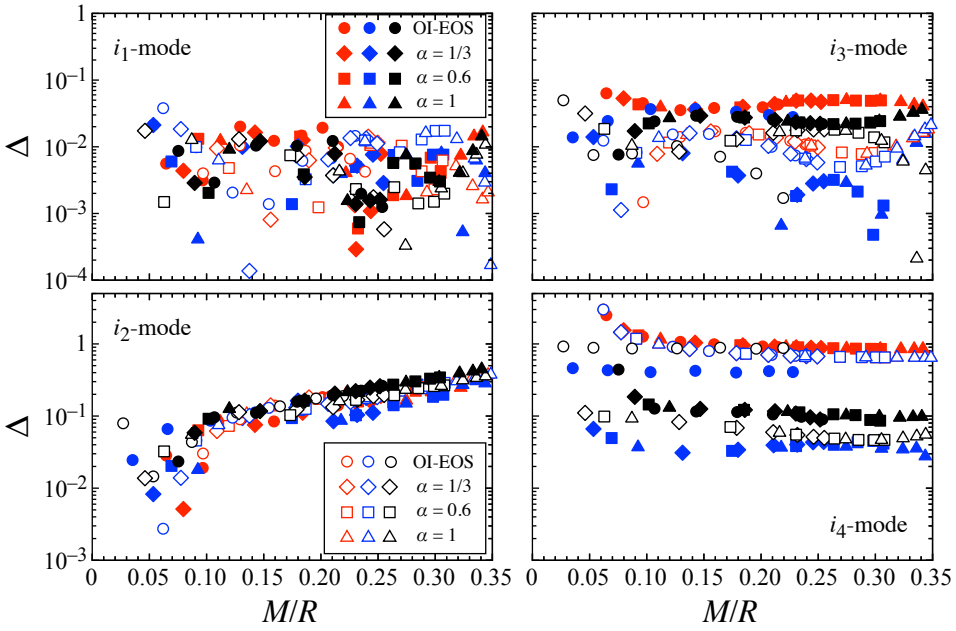


Figure 6. For the i_i-mode frequencies with $i = 1$–4, the relative deviation, Δ, using the fitting formulae given by Equations (10), (13) and (14), is shown as a function of M/R. The meaning of the marks is the same as in Figure 5. Taken from Ref. [59].

3.3. Accuracy of the Cowling Approximation

The above discussion has been done, using the *s*- and *i*-mode frequencies determined with the Cowling approximation. In this subsection, we discuss the accuracy of this approximation in the *s*- and *i*-mode frequencies by comparing the frequencies determined via the eigenvalue problem with the metric perturbations to those with the Cowling approximation [60]. As a result, we find that the *s*-mode frequencies with the Cowling approximation surprisingly agree well with those with the metric perturbations within 1% accuracy, which may come from numerical accuracy and/or marginal differences in the implementations of the numerical codes in the two approaches. In addition, we find that the eigenfunctions of the *s*-modes determined with the metric perturbations almost overlap with those with the Cowling approximation (see Figures 2 and 3 in Ref. [60]). That is, the frequencies and the corresponding eigenfunctions of *s*-modes virtually receive no impact from the Cowling approximation. Considering that the Cowling approximation overestimates the *f*-mode frequencies by ∼20% [107], this is an astonishing result. In contrast, we also find that the *i*-mode frequencies determined with the Cowling approximation deviate from those with the metric perturbations by about 20%; e.g., the Cowling approximation overestimates the i_1-mode frequency and underestimates the i_2-mode frequency, compared to the frequencies determined with the metric perturbations [60]. One also observes deviations in the corresponding eigenfunctions. Such a discrepancy in the frequencies as well as the corresponding eigenfunctions of the *i*-modes is somewhat unexpected. As the *i*-modes are very weakly coupled to the spacetime and hardly radiate gravitational waves (see the next paragraph), we would expect them to be almost unaffected by the Cowling approximation, as for the *s*-modes. While this result may be physical in nature, if it is not, we were ultimately unable to identify the cause of this discrepancy. Anyway, the deviation of the *i*-mode frequencies determined with the metric perturbations from those with the Cowling approximation is much larger than the uncertainties of the fitting formulae for the i_1-mode frequencies derived from the calculation with the Cowling approximation. In other words, to extract the physical properties under realistic situations, it is necessary to calculate the frequency of the *i*-mode using metric perturbations and to rederive the fitting formula, even

if our fitting formula for the i_1-mode frequencies derived with the Cowling approximation qualitatively represents specific characteristics of the i_1-mode (although this point itself requires verification).

As an advantage of a full relativistic approach taking into account the metric perturbations, one can discuss the damping rate of the gravitational waves. Because gravitational waves carry away energy, the stellar oscillations would damp out; i.e., the eigenfrequencies become complex, the so-called quasi-normal modes. Through a standard numerical method, we tried to determine the damping rate for the *s*- and *i*-mode oscillations, but the damping rate is too low to calculate, which is comparable to or less than the numerical accuracy. Therefore, to estimate the damping rate, we adopt two different approaches; i.e., one is the method using the ratio of the outgoing and ingoing wave amplitudes for purely real-valued frequencies [110], based on the standard Breit–Wigner resonance, and the other is the well-known quadrupole formula [108,111], using the estimation of the oscillation energy with the specific mode [111,112]. Then, we could estimate the damping time to be $\gtrsim 10^6$ s for the s_1-modes and $>10^8$ s for the i_1-modes. Thus, the damping rate of the *s*- and *i*-modes is very low, which means that the gravitational wave emissions from these modes are so weak as to be virtually negligible. We emphasize that the damping time estimated here is due to gravitational radiation alone, not necessarily the physical lifetimes of the modes, which may be affected by other dissipative or nonlinear processes.

4. Conclusions

In this article, we synthesized the results of Refs. [58–60] and discussed their implications for NS seismology. The *s*- and *i*-mode frequencies excited by the elasticity inside the neutron star are directly associated with the properties in the elastic region. In this study, we focus on the crust elasticity, even though there may exist another elastic region inside the star. The *s*- and *i*-mode frequencies might be observed in the precursor signal resulting from the resonant shattering that occurred before the main short gamma-ray burst corresponding to the merger of a binary neutron star. If observed, this would be a good opportunity to detect the gravitational waves from the neutron stars, where one could extract the neutron star properties, especially the crust properties, through the technique of asteroseismology. Nevertheless, as the excited frequencies strongly depend on uncertainties, such as neutron star mass, radius, and EOS, it may be difficult to directly obtain the physical information from the observed frequencies of gravitational waves. To solve this difficulty, we could derive the fitting formulae for the s_i-mode with $i = 1$–4 and the i_1-mode frequencies as a function of stellar compactness and the combination of the nuclear saturation parameters, K_0 and L, independently of the stiffness of the core EOS, at least when the EOS in a higher-density region can be characterized only by the specific constant sound velocity. We have to emphasize that we adopt the barotropic approximation in this manuscript; i.e., a realistic EOS with stratification may change the mode identification itself.

Our fitting formula for the elastic frequencies becomes a function of neutron star properties, i.e., the mass M and radius R, and the EOS parameters, K_0 and L, indicating that the observation of a single frequency does not directly provide a constraint on K_0 and L without additional information about the stellar parameters M and R. Even if M and R were independently known, one frequency would generally constrain a combination of the nuclear parameters rather than determine them separately. The possibility of obtaining stronger constraints from several observed modes depends on the independence of the corresponding parameter combinations, their measurement uncertainties, and the reliability of mode identification. This means that the fitting formula derived in this article provides one of the relationships in the parameter space comprising the EOS parameters and the properties of the star; by combining this with relationships obtained from entirely different

observations, it is possible to narrow down the parameter space. In such a way, one of the potential sources of the elastic oscillations considered in this article is crustal oscillations, which may emerge as a precursor before a binary neutron star merger observed as a short gamma-ray burst. Resolving these oscillation modes considered in this article is currently very difficult in observations as well as in numerical simulations. Nevertheless, should the resolution of both numerical simulations and observations improve dramatically in the future, and should frequencies arising from crustal elasticity—such as those discussed here—be observed, it may be possible to shed light on properties of the crust that remain unclear at present.

Since we consider EOS models (OI-EOS), which are characterized only by the nuclear saturation parameters, i.e., the lowest-order expansion coefficients of zero-temperature homogeneous nuclear matter in the vicinity of the saturation density of symmetric nuclear matter, our statement in this article is valid only when the correlations with the nuclear saturation parameters are well preserved. If not, additional analysis is needed to validate our statement. A useful way of verifying the robustness of our findings is to examine whether various kernel functions such as more flexible nucleonic EOS models proposed in Ref. [105]—with roughly the same saturation parameter but differing in their remaining parameters—predict equivalent elastic mode frequencies. Such an extension will be done somewhere in the future. In addition, we also have to examine the effects neglected in this article, such as neutron superfluidity and composition fraction inside the star, and/or the case without simple approximations, such as the zero shear modulus inside the slab-like nuclei. Actually, the frequencies of elastic oscillations possibly increase due to neutron superfluidity, which depends on the effective dynamical coupling between the dripped neutrons and the crust, including entrainment.

Funding: This work is supported in part by the Mitsubishi Foundation through grant No. 202510029.

Institutional Review Board Statement: Not applicable.

Informed Consent Statement: Not applicable.

Data Availability Statement: Dataset available on request from the authors.

Acknowledgments: We are grateful to Christian J. Krüger for valuable comments.

Conflicts of Interest: The author declares no conflicts of interest.

Abbreviations

The following abbreviations are used in this manuscript:

EOS Equation of state
TOV Tolman–Oppenheimer–Volkoff

Appendix A. Mass–Radius Relations

In this appendix, we show the mass–radius relations of the neutron star models considered in Figure 4. In Figure A1, the mass–radius relations for the neutron star models are shown, where the solid lines denote the stellar models constructed with the OI-EOS, while the dashed and dotted lines denote those constructed with the OI-EOS connected to the EOS given by Equation (3) in a higher-density region. For reference, astronomical constraints are also shown, i.e., NICER observations for PSR J0030+0451 [10,11] and for PSR J0740+6620 [12–14]; the gravitational waves from the binary neutron star merger, GW170817 [9]; the high-frequency QPOs from GRB 200415A [31]; and quasi-periodic oscillations from FRB 2024114A [92]. In addition to the astronomical constraints, the neutron star models, whose central density is low, can be constrained from the experimental

values of K_0 and L using the low-mass neutron star mass formula proposed in Ref. [113]. The right-bottom shaded region is such an allowed region by adopting the fiducial values of $K_0 = 240 \pm 20$ MeV [87] and $L = 60 \pm 20$ MeV [88,89]. From this figure, one can observe that the stellar models considered in Figure 4 cover a surprisingly wide range of the mass–radius plane.

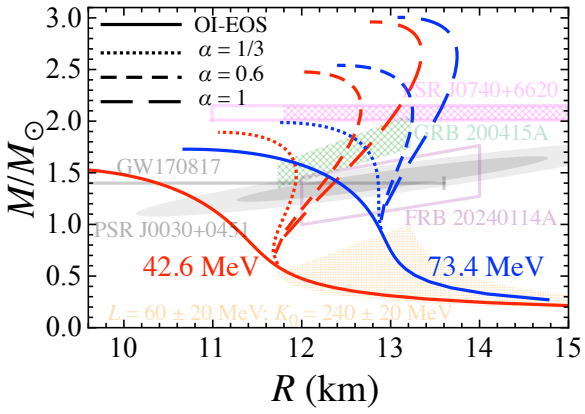


Figure A1. Mass–radius relations of the neutron star models considered in Figure 4. The solid lines denote the stellar models constructed with the OI-EOS, while the dashed and dotted lines denote those constructed with the OI-EOS connected to the EOS given by Equation (3) in a higher-density region. For reference, some of the observational constraints are also shown (see the text for the details).

Appendix B. Dependence of the Transition Density Between an Elastic Crust and the Envelope

In this study, we assume that the transition density between the surface of the spherical nuclei and the envelope is 10^{10} g/cm^3. However, if this transition density is different from this assumed value, the frequencies of the elastic oscillations, especially the i-mode frequencies, may change, depending on the transition density. In this appendix, we examine how the i-mode frequencies shift as the transition density varies. For this purpose, we simply consider the stellar models with an elastic region inside the spherical and cylindrical nuclei, while the elasticity inside the slab-like, cylindrical-hole, and spherical-hole nuclei is neglected. That is, the number of excited i-modes is only two, which can be excited at the interfaces between the surface of the spherical nuclei phase and the envelope, and between the cylindrical and slab-like nuclei phases. Here, the i_1-mode is the oscillation mode whose amplitude becomes large at both boundaries, while the i_2-mode is the mode whose amplitude mainly becomes large at the boundary between the crust and the envelope.

Then, we vary the transition density between the surface of the spherical nuclei and the envelope from 10^{12} to 10^{14} g/cm^3, focusing on the stellar model with $1.4M_\odot$ and 12.4 km constructed with the OI-EOS with $L = 73.4$ MeV and $K_0 = 230$ MeV. The corresponding change in the crust thickness is from $\Delta R = 0.503$ to 0.075 km. The behavior of the i_1- and i_2-mode frequencies is shown in Figure A2. From this figure, one can observe that i_1-mode frequencies are almost independent of the variation in the transition density between the crust and the envelope, while the i_2-mode frequencies significantly depend on it. In fact, the i_2-mode frequencies decrease and eventually disappear when the transition density increases, corresponding to the decrease in the crust thickness. In a realistic (cold) neutron star, the transition density may not be so high that we can observe a significant shift in the i-mode frequencies, but it may happen in a neutron star where the crust is just forming during neutron star cooling.

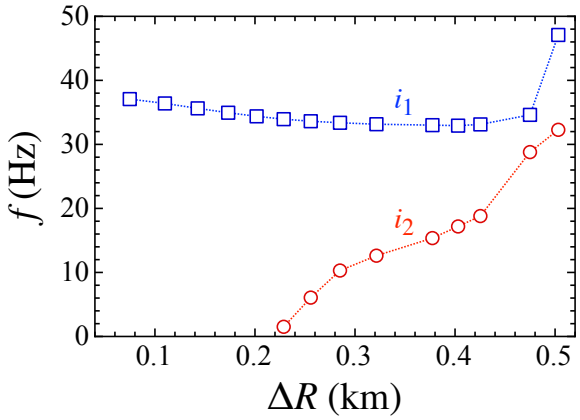


Figure A2. The dependence of the i_1- and i_2-mode frequencies on the crust thickness (or the transition density between the surface of the spherical nuclei phase and the envelope). In particular, for simplicity, the neutron star models are considered with an elastic region inside the spherical and cylindrical nuclei, where the elasticity in the slab-like, cylindrical-hole, and spherical-hole nuclei is neglected. That is, the two i-modes can be excited at the interfaces between the surface of the phase of spherical nuclei and the envelope, and between the phases of cylindrical and slab-like nuclei. The neutron star model shown here has a mass of $1.4M_\odot$ and a radius of 12.4 km, using the OI-EOS with $L = 73.4$ MeV and $K_0 = 230$ MeV. Taken from Ref. [58].

Notes

[1] According to the recent study, it has been reported that the canonical i-mode associated with the crust-core boundary vanishes in stratified neutron stars and is replaced by compositional gravity (g-) modes with mixed gravity-interfacial character, driven primarily by strong buoyancy in the outer core [48].

[2] It has been shown that, when considering the extended branch of hybrid stars in the slow transformation regime, i.e., slow stable hybrid stars, some of the proposed universal relations do not hold [81,82].

[3] As mentioned in the previous section, we construct the equilibrium model by using the EOS given by Equation (3) connected to the OI-EOS at $\varepsilon = \varepsilon_t$. So, in practice, we integrate the perturbation equations with the EOS given by Equation (3) from the center to the radial position where $\varepsilon = \varepsilon_t$, and continue integrating the perturbation equations outward with the OI-EOS.

[4] In the case that the elastic region is too narrow, the number of the excited i-modes becomes less than the number of the interface inside the star, or some of the i-mode frequencies become too low to numerically determine [58].

References

1. Shapiro, S.L.; Teukolsky, S.A. *Black Holes, White Dwarfs, and Neutron Stars: The Physics of Compact Objects*; Wiley-Interscience: New York, NY, USA, 1983.
2. Lattimer, J.M.; Prakash, M. The Physics of Neutron Stars. *Science* **2004**, *304*, 536–542. [CrossRef]
3. Demorest, P.; Pennucci, T.; Ransom, S.; Roberts, M.; Hessels, J. A two-solar-mass neutron star measured using Shapiro delay. *Nature* **2010**, *467*, 1081–1083. [CrossRef]
4. Fonseca, E.; Cromartie, H.T.; Pennucci, T.T.; Ray, P.S.; Kirichenko, A.Y.; Ransom, S.M.; Demorest, P.B.; Stairs, I.H.; Arzoumanian, Z.; Guillemot, L.; et al. Refined Mass and Geometric Measurements of the High-Mass PSR J0740+6620. *Astrophys. J.* **2021**, *915*, L12. [CrossRef]
5. Saffer, A.; Fonseca, E.; Ransom, S.; Stairs, I.; Lynch, R.; Good, D.; Masui, K.W.; McKee, J.W.; Meyers, B.W.; Patil, S.S.; et al. A Lower Mass Estimate for PSR J0348+0432 Based on CHIME/Pulsar Precision Timing. *Astrophys. J.* **2025**, *983*, L20. [CrossRef]
6. Romani, R.W.; Beleznay, M.; Filippenko, A.V.; Brink, T.G.; Zheng, W. PSR J0952-0607: Tightening a Record-high Neutron Star Mass. *Astrophys. J.* **2026**, *996*, 101. [CrossRef]
7. Abbott, B.P.; Abbott, R.; Abbott, T.D.; Acernese, F.; Ackley, K.; Adams, C.; Adams, T.; Addesso, P.; Adhikari, R.X.; Adya, V.B.; et al. GW170817: Observation of Gravitational Waves from a Binary Neutron Star Inspiral. *Phys. Rev. Lett.* **2017**, *119*, 161101. [CrossRef]
8. Abbott, B.P.; Abbott, R.; Abbott, T.D.; Acernese, F.; Ackley, K.; Adams, C.; Adams, T.; Addesso, P.; Adhikari, R.X.; Adya, V.B.; et al. Multi-messenger Observations of a Binary Neutron Star Merger. *Astrophys. J.* **2017**, *848*, L12. [CrossRef]

9. Annala, E.; Gorda, T.; Kurkela, A.; Vuorinen, A. Gravitational-Wave Constraints on the Neutron-Star-Matter Equation of State. *Phys. Rev. Lett.* **2018**, *120*, 172703. [CrossRef]
10. Riley, T.E.; Watts, A.L.; Bogdanov, S.; Ray, P.S.; Ludlam, R.M.; Guillot, S.; Arzoumanian, Z.; Baker, C.L.; Bilous, A.V.; Chakrabarty, D.; et al. A NICER View of PSR J0030+0451: Millisecond Pulsar Parameter Estimation. *Astrophys. J.* **2019**, *887*, L21. [CrossRef]
11. Miller, M.C.; Lamb, F.K.; Dittmann, A.J.; Bogdanov, S.; Arzoumanian, Z.; Gendreau, K.C.; Guillot, S.; Harding, A.K.; Ho, W.C.G.; Lattimer, J.M.; et al. PSR J0030+0451 Mass and Radius from NICER Data and Implications for the Properties of Neutron Star Matter. *Astrophys. J.* **2019**, *887*, L24. [CrossRef]
12. Riley, T.E.; Watts, A.L.; Ray, P.S.; Bogdanov, S.; Guillot, S.; Morsink, S.M.; Bilous, A.V.; Arzoumanian, Z.; Choudhury, D.; Deneva, J.S.; et al. A NICER View of the Massive Pulsar PSR J0740+6620 Informed by Radio Timing and XMM-Newton Spectroscopy. *Astrophys. J.* **2021**, *918*, L27. [CrossRef]
13. Miller, M.C.; Lamb, F.K.; Dittmann, A.J.; Bogdanov, S.; Arzoumanian, Z.; Gendreau, K.C.; Guillot, S.; Ho, W.C.G.; Lattimer, J.M.; Loewenstein, M.; et al. The Radius of PSR J0740+6620 from NICER and XMM-Newton Data. *Astrophys. J.* **2021**, *918*, L28. [CrossRef]
14. Dittmann, A.J.; Miller, M.C.; Lamb, F.K.; Holt, I.M.; Chirenti, C.; Wolff, M.T.; Bogdanov, S.; Guillot, S.; Ho, W.C.G.; Morsink, S.M.; et al. A More Precise Measurement of the Radius of PSR J0740+6620 Using Updated NICER Data. *Astrophys. J.* **2024**, *974*, 295. [CrossRef]
15. Choudhury, D.; Salmi, T.; Vinciguerra, S.; Riley, T.E.; Kini, Y.; Watts, A.L.; Dorsman, B.; Bogdanov, S.; Guillot, S.; Ray, P.S.; et al. A NICER View of the Nearest and Brightest Millisecond Pulsar: PSR J0437-4715. *Astrophys. J.* **2024**, *971*, L20. [CrossRef]
16. Mauviard, L.; Guillot, S.; Salmi, T.; Choudhury, D.; Dorsman, B.; González-Caniulef, D.; Hoogkamer, M.; Huppenkothen, D.; Kazantsev, C.; Kini, Y.; et al. A NICER View of the 1.4 $M_{\odot}$ Edge-on Pulsar PSR J0614-3329. *Astrophys. J.* **2025**, *995*, 60. [CrossRef]
17. Lattimer, J.M. Neutron Star Mass and Radius Measurements. *Universe* **2019**, *5*, 159. [CrossRef]
18. Sotani, H.; Nishimura, N.; Naito, T. New constraints on the neutron-star mass and radius relation from terrestrial nuclear experiments. *Prog. Theor. Exp. Phys.* **2022**, *2022*, 041D01. [CrossRef]
19. Sotani, H.; Ota, S. Neutron star mass formula with nuclear saturation parameters for asymmetric nuclear matter. *Phys. Rev. D* **2022**, *106*, 103005. [CrossRef]
20. Sotani, H.; Naito, T. Empirical neutron star mass formula based on experimental observables. *Phys. Rev. C* **2023**, *107*, 035802. [CrossRef]
21. Drischler, C.; Holt, J.W.; Wellenhofer, C. Chiral Effective Field Theory and the High-Density Nuclear Equation of State. *Annu. Rev. Nucl. Part. Sci.* **2021**, *71*, 403. [CrossRef]
22. Kokkotas, K.D.; Schmidt, B.G. Quasi-Normal Modes of Stars and Black Holes. *Living Rev. Relativ.* **1999**, *2*, 2. [CrossRef]
23. Andersson, N. A Gravitational-Wave Perspective on Neutron-Star Seismology. *Universe* **2021**, *7*, 97. [CrossRef]
24. Andersson, N.; Kokkotas, K.D. Gravitational Waves and Pulsating Stars: What Can We Learn from Future Observations? *Phys. Rev. Lett.* **1996**, *77*, 4134. [CrossRef]
25. Andersson, N.; Kokkotas, K.D. Towards gravitational wave asteroseismology. *Mon. Not. R. Astron. Soc.* **1998**, *299*, 1059. [CrossRef]
26. Kokkotas, K.D.; Apostolatos, T.A.; Andersson, N. The inverse problem for pulsating neutron stars: A 'fingerprint analysis' for the supranuclear equation of state. *Mon. Not. R. Astron. Soc.* **2001**, *320*, 307. [CrossRef]
27. Steiner, A.W.; Watts, A.L. Constraints on Neutron Star Crusts from Oscillations in Giant Flares. *Phys. Rev. Lett.* **2009**, *103*, 181101. [CrossRef]
28. Gearheart, M.; Newton, W.G.; Hooker, J.; Li, B.-A. Upper limits on the observational effects of nuclear pasta in neutron stars. *Mon. Not. R. Astron. Soc.* **2011**, *418*, 2343. [CrossRef]
29. Sotani, H.; Nakazato, K.; Iida, K.; Oyamatsu, K. Probing the Equation of State of Nuclear Matter via Neutron Star Asteroseismology. *Phys. Rev. Lett.* **2012**, *108*, 201101. [CrossRef]
30. Sotani, H.; Iida, K.; Oyamatsu, K. Astrophysical implications of double-layer torsional oscillations in a neutron star crust as a lasagna sandwich. *Mon. Not. R. Astron. Soc.* **2019**, *489*, 3022. [CrossRef]
31. Sotani, H.; Kokkotas, K.D.; Stergioulas, N. Neutron star mass-radius constraints using the high-frequency quasi-periodic oscillations of GRB 200415A. *Astron. Astrophys.* **2023**, *676*, A65. [CrossRef]
32. Sotani, H. Magnetar QPOs and neutron star crust elasticity. *Universe* **2024**, *10*, 231. [CrossRef]
33. Sotani, H.; Yasutake, N.; Maruyama, T.; Tatsumi, T. Signatures of hadron-quark mixed phase in gravitational waves. *Phys. Rev. D* **2011**, *83*, 024014. [CrossRef]
34. Gaertig, E.; Kokkotas, K.D. Gravitational wave asteroseismology with fast rotating neutron stars. *Phys. Rev. D* **2011**, *83*, 064031. [CrossRef]
35. Passamonti, A.; Andersson, N. Towards real neutron star seismology: Accounting for elasticity and superfluidity. *Mon. Not. R. Astron. Soc.* **2012**, *419*, 638. [CrossRef]
36. Doneva, D.D.; Gaertig, E.; Kokkotas, K.D.; Krüger, C. Gravitational wave asteroseismology of fast rotating neutron stars with realistic equations of state. *Phys. Rev. D* **2013**, *88*, 044052. [CrossRef]

37. Sotani, H. Neutron star asteroseismology and nuclear saturation parameter. *Phys. Rev. D* **2021**, *103*, 123015. [CrossRef]
38. Fuller, J.; Klion, H.; Abdikamalov, E.; Ott, C.D. Supernova seismology: Gravitational wave signatures of rapidly rotating core collapse. *Mon. Not. R. Astron. Soc.* **2015**, *450*, 414. [CrossRef]
39. Morozova, V.; Radice, D.; Burrows, A.; Vartanyan, D. The Gravitational Wave Signal from Core-Collapse Supernovae. *Astrophys. J.* **2018**, *861*, 10. [CrossRef]
40. Torres-Forné, A.; Cerdá-Durán, P.; Passamonti, A.; Font, J.A. Towards asteroseismology of core-collapse supernovae with gravitational-wave observations—I. Cowling approximation. *Mon. Not. R. Astron. Soc.* **2018**, *474*, 5272. [CrossRef]
41. Sotani, H.; Takiwaki, T.; Togashi, H. Universal relation for supernova gravitational waves. *Phys. Rev. D* **2021**, *104*, 123009. [CrossRef]
42. Jakobus, P.; Müller, B.; Heger, A.; Zha, S.; Powell, J.; Motornenko, A.; Steinheimer, J.; Stöcker, H. Gravitational Waves from a Core g Mode in Supernovae as Probes of the High-Density Equation of State. *Phys. Rev. Lett.* **2023**, *131*, 191201. [CrossRef]
43. Sotani, H.; Müller, B.; Takiwaki, T. Effects of multidimensional treatment of gravity in simulations on supernova gravitational waves. *Phys. Rev. D* **2025**, *112*, 083018. [CrossRef]
44. Sotani, H. Understanding supernova gravitational waves with protoneutron star asteroseismology. *Class. Quantum Gravity* **2026**, *43*, 093001. [CrossRef]
45. Pereira, J.P.; Flores, C.V.; Lugones, G. Phase Transition Effects on the Dynamical Stability of Hybrid Neutron Stars. *Astrophys. J.* **2018**, *860*, 12. [CrossRef]
46. Gonçalves, V.P.; Lazzari, L. Impact of slow conversions on hybrid stars with sequential QCD phase transitions. *Eur. Phys. J. C* **2022**, *82*, 288. [CrossRef]
47. Chamel, N.; Haensel, P. Physics of Neutron Star Crusts. *Living Rev. Relativ.* **2008**, *11*, 10. [CrossRef]
48. Gao, Y.; Kuan, H.-J.; Xia, C.-J.; Silva, H.O.; Shibata, M. Nonradial oscillations of stratified neutron stars with solid crusts: Mode characterization and tidal resonances in coalescing binaries. *Phys. Rev. D* **2025**, *112*, 123006. [CrossRef]
49. Bastrukov, S.I.; Molodtsova, I.V.; Papoyan, V.V.; Weber, F. Non-radial vibrations of neutron stars. *J. Phys. G Nucl. Part. Phys.* **1996**, *22*, L33. [CrossRef]
50. Bastrukov, S.I.; Libert, J.; Molodtsova, I.V. Elastodynamic Features of Nuclear Matter from Macroscopic Model of Giant Magnetic Resonances. *Int. J. Mod. Phys. E* **1997**, *6*, 89–110. [CrossRef]
51. Bastrukov, S.I.; Weber, F.; Podgainy, D.V. On the stability of global non-radial pulsations of neutron stars. *J. Phys. G Nucl. Part. Phys.* **1999**, *25*, 107. [CrossRef]
52. Bastrukov, S.I.; Papoyan, V.V.; Podgainy, D.V. Stratified model of a neutron star. *Astrophysics* **1999**, *42*, 177–189. [CrossRef]
53. Stergioulas, N. Rotating Stars in Relativity. *Living Rev. Relativ.* **1998**, *1*, 8. [CrossRef]
54. Finn, L.S. Non-radial pulsations of neutron stars with a crust. *Mon. Not. R. Astron. Soc.* **1990**, *245*, 82. [CrossRef]
55. Yoshida, S.; Lee, U. Nonradial oscillations of neutron stars with a solid crust—Analysis in the relativistic Cowling approximation. *Astron. Astrophys.* **2002**, *395*, 201–208.
56. Piro, A.L.; Bildsten, L. Neutron Star Crustal Interface Waves. *Astrophys. J.* **2005**, *619*, 1054. [CrossRef]
57. Krüger, C.J.; Ho, W.C.G.; Andersson, N. Seismology of adolescent neutron stars: Accounting for thermal effects and crust elasticity. *Phys. Rev. D* **2015**, *92*, 063009. [CrossRef]
58. Sotani, H. Shear and interface modes in neutron stars with pasta structures. *Phys. Rev. D* **2023**, *107*, 123025. [CrossRef]
59. Sotani, H. Shear oscillations in neutron stars and the nuclear symmetry energy. *Phys. Rev. D* **2024**, *109*, 023030. [CrossRef]
60. Krüger, C.J.; Sotani, H. Impact of the relativistic Cowling approximation on shear and interface modes of neutron stars. *Phys. Rev. D* **2025**, *111*, 063029. [CrossRef]
61. Lai, D. Resonant oscillations and tidal heating in coalescing binary neutron stars. *Mon. Not. R. Astron. Soc.* **1994**, *270*, 611–629. [CrossRef]
62. Reisenegger, A.; Goldreich, P. Excitation of Neutron Star Normal Modes during Binary Inspiral. *Astrophys. J.* **1994**, *426*, 688. [CrossRef]
63. Abbott, B.P.; Adya, V.B.; Affeldt, C.; Agarwal, B.; Agathos, M.; Agatsuma, K.; Aggarwal, N.; Aguiar, O.D.; Aiello, L.; Ain, A.; et al. Constraining the p-Mode–g-Mode Tidal Instability with GW170817. *Phys. Rev. Lett.* **2019**, *122*, 061104. [CrossRef]
64. Kuan, H.-J.; Suvorov, A.G.; Kokkotas, K.D. General-relativistic treatment of tidal g-mode resonances in coalescing binaries of neutron stars - I. Theoretical framework and crust breaking. *Mon. Not. R. Astron. Soc.* **2021**, *506*, 2985–2998. [CrossRef]
65. Kuan, H.-J.; Kiuchi, K.; Shibata, M. Tidal Resonance in Binary Neutron Star Inspirals: A High-Precision Study in Numerical Relativity. *Phys. Rev. Lett.* **2025**, *135*, 141403. [CrossRef]
66. Tsang, D.; Read, J.S.; Hinderer, T.; Piro, A.L.; Bondarescu, R. Resonant Shattering of Neutron Star Crust. *Phys. Rev. Lett.* **2012**, *108*, 011102. [CrossRef]
67. Tsang, D. Shattering Flares during Close Encounters of Neutron Stars. *Astrophys. J.* **2013**, *777*, 103. [CrossRef]
68. Gittins, F.; Andersson, N.; Pereira, J.P. Tidal deformations of neutron stars with elastic crusts. *Phys. Rev. D* **2020**, *101*, 103025. [CrossRef]

69. Suvorov, A.G.; Kuan, H.J.; Kokkotas, K.D. Quasi-periodic oscillations in precursor flares via seismic aftershocks from resonant shattering. *Astron. Astrophys.* **2022**, *664*, A177. [CrossRef]
70. Troja, E.; Rosswog, S.; Gehrels, N. Precursors of Short Gamma-Ray Bursts. *Astrophys. J.* **2010**, *723*, 1711. [CrossRef]
71. Coppin, P.; de Vries, K.D.; van Eijndhoven, N. Identification of gamma-ray burst precursors in Fermi-GBM bursts. *Phys. Rev. D* **2020**, *102*, 103014. [CrossRef]
72. Xiao, S.; Zhang, Y.-Q.; Zhu, Z.-P.; Xiong, S.-L.; Gao, H.; Xu, D.; Zhang, S.-N.; Peng, W.-X.; Li, X.-B.; Zhang, P.; et al. The Peculiar Precursor of a Gamma-Ray Burst from a Binary Merger Involving a Magnetar. *Astrophys. J.* **2024**, *970*, 6. [CrossRef]
73. Neill, D.; Newton, W.G.; Tsang, D. Resonant shattering flares as multimessenger probes of the nuclear symmetry energy. *Mon. Not. R. Astron. Soc.* **2021**, *504*, 1129–1143. Correction in *Mon. Not. R. Astron. Soc.* **2022**, *513*, 310. [CrossRef]
74. Neill, D.; Tsang, D.; van Eerten, H.; Ryan, G.; Newton, W.G. Resonant shattering flares in black hole-neutron star and binary neutron star mergers. *Mon. Not. R. Astron. Soc.* **2022**, *514*, 5385–5402. [CrossRef]
75. Tsui, L.K.; Leung, P.T. Universality in quasi-normal modes of neutron stars. *Mon. Not. R. Astron. Soc.* **2005**, *357*, 1029–1037. [CrossRef]
76. Chirenti, C.; de Souza, G.H.; Kastaun, W. Fundamental oscillation modes of neutron stars: Validity of universal relations. *Phys. Rev. D* **2015**, *91*, 044034. [CrossRef]
77. Sotani, H.; Kumar, B. Universal relations between the quasinormal modes of neutron star and tidal deformability. *Phys. Rev. D* **2021**, *104*, 123002. [CrossRef]
78. Ranea-Sandoval, I.F.; Mariani, M.; Lugones, G.; Guilera, O.M. Constraining mass, radius, and tidal deformability of compact stars with axial wI modes: New universal relations including slow stable hybrid stars. *Mon. Not. R. Astron. Soc.* **2023**, *519*, 3194–3200. [CrossRef]
79. Guedes, V.; Lau, S.Y.; Chirenti, C.; Yagi, K. Broadening of universal relations at the birth and death of a neutron star. *Phys. Rev. D* **2024**, *109*, 083040. [CrossRef]
80. Sotani, H. Universal relations between the quasinormal modes of neutron stars and magnetic tidal deformability. *Phys. Rev. D* **2026**, *113*, 023017. [CrossRef]
81. Ranea-Sandoval, I.F.; Guilera, O.M.; Mariani, M.; Lugones, G. Breaking of universal relationships of axial *w*I modes in hybrid stars: Rapid and slow hadron-quark conversion scenarios. *Phys. Rev. D* **2022**, *106*, 043025. [CrossRef]
82. Ranea-Sandoval, I.F.; Mariani, M.; Celi, M.O.; Rodríguez, M.C.; Tonetto, L. Asteroseismology using quadrupolar f-modes revisited: Breaking of universal relationships in the slow hadron-quark conversion scenario. *Phys. Rev. D* **2023**, *107*, 123028. [CrossRef]
83. Oyamatsu, K.; Iida, K. Saturation of Nuclear Matter and Radii of Unstable Nuclei. *Prog. Theor. Phys.* **2003**, *109*, 631–650. [CrossRef]
84. Oyamatsu, K.; Iida, K. The symmetry energy at subnuclear densities and nuclei in neutron star crusts. *Phys. Rev. C* **2007**, *75*, 015801. [CrossRef]
85. Cai, B.-J.; Chen, L.-W. Nuclear matter fourth-order symmetry energy in the relativistic mean field models. *Phys. Rev. C* **2012**, *85*, 024302. [CrossRef]
86. Togashi, H.; Takano, M. Variational study for the equation of state of asymmetric nuclear matter at finite temperatures. *Nucl. Phys. A* **2013**, *902*, 53–73. [CrossRef]
87. Shlomo, S.; Kolomietz, V.M.; Colò, G. Deducing the Nuclear-Matter Incompressibility Coefficient from Data on Isoscalar Compression Modes. *Eur. Phys. J. A* **2006**, *30*, 23–30. [CrossRef]
88. Viñas, X.; Centelles, M.; Roca-Maza, X.; Warda, M. Density dependence of the symmetry energy from neutron skin thickness in finite nuclei. *Eur. Phys. J. A* **2014**, *50*, 27. [CrossRef]
89. Li, B.A.; Krastev, P.G.; Wen, D.H.; Zhang, N.B. Towards understanding astrophysical effects of nuclear symmetry energy. *Eur. Phys. J. A* **2019**, *55*, 117. [CrossRef]
90. Lattimer, J.M.; Lim, Y. Constraining the Symmetry Parameters of the Nuclear Interaction. *Astrophys. J.* **2013**, *771*, 51. [CrossRef]
91. Lattimer, J.M.; Steiner, A.W. Constraints on the symmetry energy using the mass-radius relation of neutron stars. *Eur. Phys. J. A* **2014**, *50*, 40. [CrossRef]
92. Sotani, H.; Wadiasingh, Z.; Chirenti, C. Estimation of the Neutron Star Mass and Radius of FRB 20240114A by Identification of Crustal Oscillations. *Astrophys. J.* **2026**, *1001*, L18. [CrossRef]
93. Tews, I.; Krüger, T.; Hebeler, K.; Schwenk, A. Neutron Matter at Next-to-Next-to-Next-to-Leading Order in Chiral Effective Field Theory. *Phys. Rev. Lett.* **2013**, *110*, 032504. [CrossRef]
94. Le Fèvre, A.; Leifels, Y.; Reisdorf, W.; Aichelin, J.; Hartnack, C. Constraining the nuclear matter equation of state around twice saturation density. *Nucl. Phys. A* **2016**, *945*, 112–133. [CrossRef]
95. Tews, I.; Margueron, J.; Reddy, S. Confronting gravitational-wave observations with modern nuclear physics constraints. *Eur. Phys. J. A* **2019**, *55*, 97. [CrossRef]
96. Kunjipurayil, A.; Piekarewicz, J. Thermodynamic versus dynamical description of the neutron-star crust-core instability: Implications for crustal observables. *Phys. Rev. C* **2026**, *114*, 045801. [CrossRef]
97. Gudmundsson, E.H.; Pethick, C.J.; Epstein, R.I. Structure of neutron star envelopes. *Astrophys. J.* **1983**, *272*, 286–300. [CrossRef]

98. Hernquist, L.; Applegate, J.H. Analytical models of neutron star envelopes. *Astrophys. J.* **1984**, *287*, 244–254. [CrossRef]
99. Beznogov, M.V.; Potekhin, A.Y.; Yakovlev, D.G. Heat blanketing envelopes of neutron stars. *Phys. Rept.* **2021**, *919*, 1. [CrossRef]
100. Epstein, R.I. Acoustic Properties of Neutron Stars. *Astrophys. J.* **1988**, *333*, 880–894. [CrossRef]
101. Ogata, S.; Ichimaru, S. First-principles calculations of shear moduli for Monte Carlo-simulated Coulomb solids. *Phys. Rev. A* **1990**, *42*, 4867–4870. [CrossRef]
102. Strohmayer, T.; van Horn, H.M.; Ogata, S.; Iyetomi, H.; Ichimaru, S. The shear modulus of the neutron star crust and nonradial oscillations of neutron stars. *Astrophys. J.* **1991**, *375*, 679–686. [CrossRef]
103. Pethick, C.J.; Potekhin, A.Y. Liquid crystals in the mantles of neutron stars. *Phys. Lett. B* **1998**, *427*, 7–12. [CrossRef]
104. Klausner, P.; Antonelli, M.; Gulminelli, F. Properties of the neutron star crust informed by nuclear structure data. *Phys. Rev. C* **2026**, *113*, 025808. [CrossRef]
105. Montefusco, G.; Antonelli, M.; Gulminelli, F. An Asymptotically Causal Metamodel for Neutron Star Equations of State. *arXiv* **2026**, arXiv:2604.00196.
106. McDermott, P.N.; van Horn, H.M.; Hansen, C.J. Nonradial oscillations of neutron stars. *Astrophys. J.* **1998**, *325*, 725–748. [CrossRef]
107. Yoshida, S.; Kojima, Y. Accuracy of the relativistic Cowling approximation in slowly rotating stars. *Mon. Not. R. Astron. Soc.* **1997**, *289*, 117–122. [CrossRef]
108. Thorne, K.S. Nonradial Pulsation of General-Relativistic Stellar Models. IV. The Weak-Field Limit. *Astrophys. J.* **1969**, *158*, 997–1019. [CrossRef]
109. Sotani, H.; Nakazato, K.; Iida, K.; Oyamatsu, K. Effect of superfluidity on neutron star crustal oscillations. *Mon. Not. R. Astron. Soc.* **2013**, *428*, L21–L25. [CrossRef]
110. Andersson, N.; Comer, G.L.; Langlois, D. Oscillations of general relativistic superfluid neutron stars. *Phys. Rev. D* **2002**, *66*, 104002. [CrossRef]
111. Lioutas, G.; Stergioulas, N. Universal and approximate relations for the gravitational-wave damping timescale of f-modes in neutron stars. *Gen. Relativ. Gravit.* **2018**, *50*, 12. [CrossRef]
112. Thorne, K.S. Nonradial Pulsation of General-Relativistic Stellar Models. III. Analytic and Numerical Results for Neutron Stars. *Astrophys. J.* **1969**, *158*, 1. [CrossRef]
113. Sotani, H.; Iida, K.; Oyamatsu, K.; Ohnishi, A. Mass and radius formulas for low-mass neutron stars. *Prog. Theor. Exp. Phys.* **2014**, *2014*, 051E01. [CrossRef]

Disclaimer/Publisher's Note: The statements, opinions and data contained in all publications are solely those of the individual author(s) and contributor(s) and not of MDPI and/or the editor(s). MDPI and/or the editor(s) disclaim responsibility for any injury to people or property resulting from any ideas, methods, instructions or products referred to in the content.